J. Phys.: Condens. Matter **21** (2009) 195602 (10pp) doi:10.1088/0953-8984/21/19/195602

Electronic structure of pyrochlore $Cd_2Re_2O_7$

Shih-Wen Huang[1,2], Horng-Tay Jeng[3,4], J-Y Lin[5], W J Chang[2], J M Chen[1], G H Lee[6], H Berger[7], H D Yang[8] and Keng S Liang[1,2]

[1] National Synchrotron Radiation Research Center, Hsinchu 300, Taiwan
[2] Department of Electrophysics, National Chiao Tung University, Hsinchu 300, Taiwan
[3] Institute of Physics, Academia Sinica, Taipei 11529, Taiwan
[4] Department of Physics, National Tsing Hua University, Hsinchu 300, Taiwan
[5] Institute of Physics, National Chiao Tung University, Hsinchu 300, Taiwan
[6] Instrumentation Center, National Taiwan University, Taipei 115, Taiwan
[7] Ecole Polytechnique Fédérale de Lausanne (EPFL), Lausanne, CH-1015, Switzerland
[8] Department of Physics, National Sun Yat-Sen University, Kaohsiung 804, Taiwan

E-mail: jeng@phys.sinica.edu.tw (H-T Jeng) and ago@cc.nctu.edu.tw (J-Y Lin)

Received 19 November 2008, in final form 3 March 2009
Published 16 April 2009
Online at stacks.iop.org/JPhysCM/21/195602

Abstract

Detailed band structure calculations have been performed for $Cd_2Re_2O_7$ in high-, middle- and low-temperature (T) phases. The calculations are based on the observed lattice structures from x-ray diffraction measurements. The spin–orbit interaction is incorporated self-consistently in both the generalized gradient approximation (GGA) and the GGA plus Hubbard U (GGA + U) approaches. It is found that the on-site U has negligible effects on the Re 5d band structures; therefore both the GGA and GGA + U Re 5d band energies agree well with the observed O K-edge x-ray absorption spectroscopy (XAS) spectrum, whereas the Cd 4d band energy observed from photoemission spectroscopy can only be correctly reproduced by GGA + U calculations, indicating the relatively itinerant Re 5d and localized Cd 4d electrons. On the other hand, the spin–orbit coupling gives rise to nontrivial spin and orbital magnetic moments for the middle-T phase. Most unexpectedly, we found that the low-T phase exhibits quasi-two-dimensional Fermi surfaces. The calculated carrier numbers for the three phases are, at least qualitatively, consistent with the measured Hall coefficient.

1. Introduction

Pyrochlore oxides are one of the largest structural groups among transition-metal oxides with the chemical formula $A_2B_2O_7$ or $A_2B_2O_6O'$, where B is a transition-metal cation and A is a rare-earth-metal or post-transition-metal cation. As shown in figure 1, the A-site ion is eightfold-coordinated with six O and two O′ anions forming a distorted cube. The sixfold-coordinated octahedra BO_6 form a three-dimensional corner-sharing network surrounding the A-site cations. Both the A and B sublattices reside on corner-sharing tetrahedra interpenetrating with each other, resulting in the well-known geometrically frustrated lattice and many novel phenomena [1–11].

$Cd_2Re_2O_7$, a member of the pyrochlore oxides, has attracted increasing attention and has been investigated extensively recently. It is the first superconductor found in pyrochlore oxides with a transition temperature of ∼1 K and with type-II superconductivity [4–6]. In the normal state, $Cd_2Re_2O_7$ is a rather poor metal near room temperature, showing an almost flat resistivity from 400 to 200 K [4, 5, 12]. Both the resistivity and magnetic susceptibility drop abruptly below 200 K [12]. The x-ray diffraction, resistivity, specific heat and thermoelectric power measurements on $Cd_2Re_2O_7$ single crystals all show that there exist anomalies near the second-order phase transition temperature at 200 K [4, 7, 12–14]. $Cd_2Re_2O_7$ undergoes another first-order phase transition at 120 K [15, 16], while it was also proposed that this phase transition is driven by crystal imperfection [17].

The above-mentioned phase transitions are also accompanied by structural changes. At room temperature, it crystallizes in an fcc lattice with space group of $Fd\bar{3}m$ [18]. The structure changes from cubic to tetragonal ($I\bar{4}m2$) below 200 K, and

 © 2009 IOP Publishing Ltd Printed in the UK

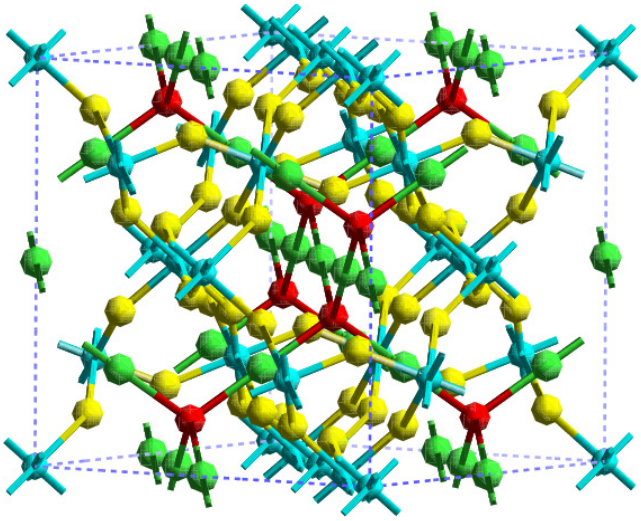

Figure 1. Lattice structure of high temperature $Cd_2Re_2O_7$. The green, blue, yellow and red spheres denote the Cd, Re, O and O′ atoms, respectively.

further to another tetragonal lattice ($I4_122$) below 120 K [19]. Meanwhile, Re nuclear quadrupole resonance (NQR) spectra [8, 20–22] reveal neither magnetic orders nor nonuniform charge distribution through all the phases.

Previous band structure calculations of the high-T cubic phase indicated that it was a semi-metal with the Fermi surfaces consisting of Re 5d electron pockets around the Γ point and hole pockets at the K point [23, 24]. The electronic structure near the Fermi level (Ef) is sensitive to the deformation of the crystal lattice [24], though the structural changes are indeed small. Spin–orbit interaction also significantly affects the electronic structures, especially in the vicinity of the Fermi level [23, 24]. The better consistency between the observed Hall coefficient [6] and calculated Fermi surface [23, 24] indicates the importance of spin–orbit coupling in $Cd_2Re_2O_7$.

By means of the electrical resistivity and Hall measurements, a large mass enhancement was observed, suggesting that an anomalous correlation plays an important role in $Cd_2Re_2O_7$ [8]. Optical spectra, revealing heavy-fermion behavior, also indicates the importance of electron correlations in this system [25]. Theoretical calculations using the local-density approximation (LDA) demonstrate that the mass enhancement is more than 5, and the low carrier and less dispersion lead $Cd_2Re_2O_7$ to a strongly correlated electron system [24]. Photoemission spectroscopy (PES) also illustrates a well-localized Cd 4d band at ∼11 eV below Ef [26], which is about 3 eV deeper than that from LDA calculations, implying that the on-site Coulomb repulsion should be take into consideration in theoretical calculations.

In this work, we conducted the x-ray diffraction measurements at different temperatures to resolve the lattice structures in three phases. Based on the observed lattice structures, we performed detailed band structure calculations for $Cd_2Re_2O_7$ in the high-T phase (>200 K), middle-T phase (120–200 K) and low-T phase (<120 K) using the generalized gradient approximation (GGA) and GGA plus Hubbard U (GGA + U) methods with spin–orbit coupling included self-consistently. The O K-edge x-ray absorption spectroscopy (XAS) was used to probe the electronic structure of the high-T phase. We also measured the T-dependent Hall coefficient from 2 to 300 K. The experimental and computational details are presented in section 2. The results are discussed in detail in section 3. The conclusions are given in section 4.

2. Experiments and methods of calculations

O K-edge XAS spectra were measured at the high-energy spherical grating monochromator beamline (HSGM) of the National Synchrotron Radiation Research Center, Taiwan. O K-edge x-ray absorption near-edge structural (XANES) spectra were obtained using the x-ray fluorescence yield method. The x-ray fluorescence yield spectra were recorded using a microchannel plate (MCP) detector, which is composed of a dual set of MCP with an electrical grid mounted in front of them. During the x-ray fluorescence yield measurements, the grid was set to a voltage of 50 V, while the front of the MCP was set to around −3200 V. The negative MCP bias was applied to expel electrons while the positive grid bias was applied to ensure that no positive ions were detected. The energy resolution of the HSGM beamline was set to ∼0.22 eV for the O K-edge x-ray absorption measurements. All the absorption spectra were processed with self-absorption correction and normalized in the range of 600–620 eV. The temperature-dependent Hall coefficient $R_H(T)$ was determined by $(\rho_{xy}(T, H = 3\ \mathrm{T})–\rho_{xy}(T, H = -3\ T))/2$ with T from 2 to 300 K. Details of the measurements for $R_H(T)$ and other transport properties will be reported elsewhere [27].

The electronic structure calculations for the three lattice structures were performed using the accurate full-potential augmented wave method [28] as implemented in the VASP package [29] within the GGA [30] and GGA + U [31, 32] schemes at 0 K. The on-site Coulomb energy U = 5.0 and 3.0 eV and the exchange parameter J = 0.6 and 0.5 eV [33] were used for Cd and Re, respectively. The lattice structures of the high-, middle- and low-T phases are in different symmetries of cubic, tetragonal and tetragonal, respectively. To achieve a better comparison, the common tetragonal lattice with four formula units (44 atoms) per unit cell was used for all three phases in this work. The calculations were performed over an 8 × 8 × 6 Monkhorst–Pack k-point mesh in the irreducible Brillouin zone with spin–orbit interaction incorporated in the self-consistent calculations under fully lattice optimizations.

3. Results and discussion

3.1. Lattice structure, spectroscopy and magnetic moment

Table 1 lists the measured atomic positions of single-crystal $Cd_2Re_2O_7$ at 295, 160 and 90 K. The space groups of the three phases used in the lattice parameter analysis are the same as those given by [18] and [19]. Our measured lattice parameters and those from [19] both indicate very slight changes ($\lesssim$1%)

Table 1. Atomic coordinates of $Cd_2Re_2O_7$ measured at 295 K (top panel), 160 K (middle panel) and 90 K (bottom panel).

		x	y	z
295 K ($Fd\bar{3}m$), $a = b = c = 10.2261(5)$ Å				
Re	16c	0.2500	0.7500	0.5000
Cd	16d	0.5000	0.5000	0.5000
O(1)	48f	0.3152(9)	0.6250	0.6250
O(2)	8b	0.6250	0.6250	0.6250
160 K ($I\bar{4}m2$), $a = b = 7.2312(3)$ Å, $c = 10.2257(4)$ Å				
Re	8i	0.2471(2)	0.0000	0.872 94(15)
Cd	8i	0.0000	0.2471(4)	0.6259(3)
O(1)	8h	0.3059(15)	0.1941(15)	0.7500
O(2)	4e	0.0000	0.0000	0.8026(16)
O(3)	8g	0.1889(16)	0.1889(16)	0.0000
O(4)	4f	0.5000	0.0000	0.9317(19)
O(5)	2b	0.0000	0.0000	0.5000
O(6)	2d	0.0000	0.5000	0.7500
90 K ($I4_122$), $a = b = 7.2313(4)$ Å, $c = 10.2282(6)$ Å				
Re	8f	0.2500	0.9967(3)	0.8750
Cd	8f	0.5041(6)	0.2500	0.1250
O(1)	8d	0.1880(20)	0.1880(20)	0.0000
O(2)	8c	0.5000	0.0000	0.9396(14)
O(3)	8e	0.1970(20)	0.8030(20)	0.0000
O(4)	4b	0.5000	0.5000	0.0000

in the lattice structures upon varying temperatures. As can be seen in the table, the changes in the lattice constants of the three phases are negligible (less than 0.02%). The Re–O bond lengths are about 1.93 Å with a typical deviation less than 0.5% among different phases, while the bond lengths of Cd–O and Cd–O′ are about 2.62 Å and 2.21 Å, respectively, with changes of ∼1% for the long Cd–O bonds and less than 0.02% for the short Cd–O′ bonds upon varying temperatures.

It has been discussed in [23] that the internal lattice parameter $x = 0.309$ of the high-T phase from earlier measurement [18] yields rather short Re–O bond lengths of ∼1.90 Å. With the lattice constant fixed, they obtained the optimized x of 0.316 [23], which is much closer to $x = 0.319$ from a newer measurement [19]. Under full lattice structure relaxation, we also obtain a higher x of 0.318 for the high-T phase with Re–O bond lengths of ∼1.92 Å. We note here that our optimized lattice parameters for the three phases differ from our measured ones by the order of 1%, which is a typical deviation between experimental and theoretical lattice parameters.

Figure 2(a) presents high-T O K-edge x-ray absorption spectra of single-crystalline $Cd_2Re_2O_7$ measured at 300 K as well as the photo-emission spectra (PES) from [26]. The calculated total density of states (DOS) from GGA and GGA+U based on the optimized lattice structure for the high-T phase are depicted in figures 2(b) and (c), respectively. The contributions from O p states are also depicted for a comparison with the O K-edge XAS spectrum. The XAS spectrum from 525 to 550 eV (figure 2(a)) shows several main features: a peak near the threshold (∼530 eV), a peak at ∼534 eV, a broad band from ∼534 to ∼540 eV and a band at ∼543 eV. Meanwhile, the PES illustrates a peak at Ef, a plateau from ∼3 to ∼10 eV below Ef and a localized band at ∼−11 eV. In comparison with the calculated DOS (figures 2(b) and (c)), one can find good correspondences between the experimental spectra and the theoretical band dispersions. As indicated in figure 2(a), partial DOS analysis demonstrates that the XAS structure near the threshold (∼530 eV) corresponds to the Re t_{2g} band, the peak at ∼534 eV comes from the Cd 5s state, the broad band from ∼534 to ∼540 eV is contributed from Re e_g and Cd 5p, and the feature at about 543 eV belongs to the Re 6s and Cd 5p bands. On the other hand, the PES peak right below Ef also corresponds to the partially filled itinerant Re t_{2g} band, the plateau from ∼−3 to ∼−10 eV comes from the O 2p band and the band at ∼−11 eV represents the localized Cd 4d band.

One of the interesting issues is what kind of role the Coulomb repulsion U plays in $Cd_2Re_2O_7$. As can be seen in figure 2, all the unoccupied bands and the partially occupied Re t_{2g} band from XAS and GGA as well as from GGA + U agree well with each other. The on-site electron correlation U has only negligible effect on the Re 5d bands so that the obtained DOS from GGA and GGA + U are nearly the same, indicating the itinerant character of the relatively delocalized Re 5d orbitals. This is also the case in the middle- and low-T phases (figures 3 and 4). Meanwhile, the occupied O 2p band energies from both GGA and GGA + U are also similar to the PES lineshape. However, there exist significant deviations in the energy of Cd 4d states between GGA and GGA + U results. Figure 2(b) shows that the Cd 4d band from GGA is located at about 8 eV below Ef. By taking into consideration the on-site electron Coulomb repulsion U of 5 eV for Cd [33], the Cd 4d bands are strongly pushed down to a lower energy of ∼−10 eV (figure 2(c)), which is compatible with the PES binding energy of about 11 eV [26] (figure 2(a)). A higher value of $U = 7$ eV would further lower this band energy to about 11 eV, leading to a better agreement with experimental results. We note here that not all oxides are strongly correlated materials. Furthermore, not all species in a compound show strong correlations. By using the GGA + U method in this work, we clarify that the Hubbard U has totally different effects on the two composed elements in $Cd_2Re_2O_7$ because of the relatively localized closed shell Cd^{2+} 4d orbitals where the Coulomb repulsion is much stronger than that in the partially filled metallic Re^{5+} 5d orbitals, which is actually weakly correlated.

Figure 3 shows the partial density of states of Cd and Re for three different phases from both GGA and GGA + U. The obtained high-T results (top panels) from GGA agree well with those reported in previous works [23, 24]. The closed shell Cd^{2+} 4d band is located at ∼8 eV below Ef, while the Fermi level lies in the partially filled Re^{5+} t_{2g} band with the octahedral crystal field splitting between this band and the higher lying e_g band being about 5 eV. For all the three phases, the on-site U narrows the Cd 4d bandwidth and pushes this band towards a lower energy closer to the observed PES binding energy [26], while it has no noticeable effect on the Re 5d band. Through the phase transitions, the DOS of Cd remain to be about the same, while there are changes

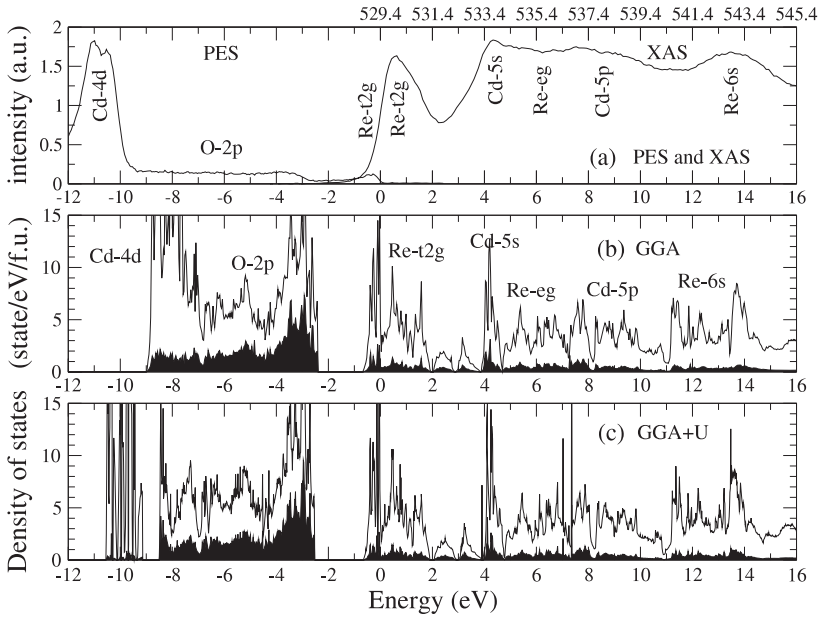

Figure 2. (a) PES [26] and O 1s XAS (this work) spectra of $Cd_2Re_2O_7$. The Fermi level of XAS is at 529.4 eV (reflection point method). (b) Total density of states from GGA (b) and GGA + U (c). The dark area in (b) and (c) are the contributions from O p states.

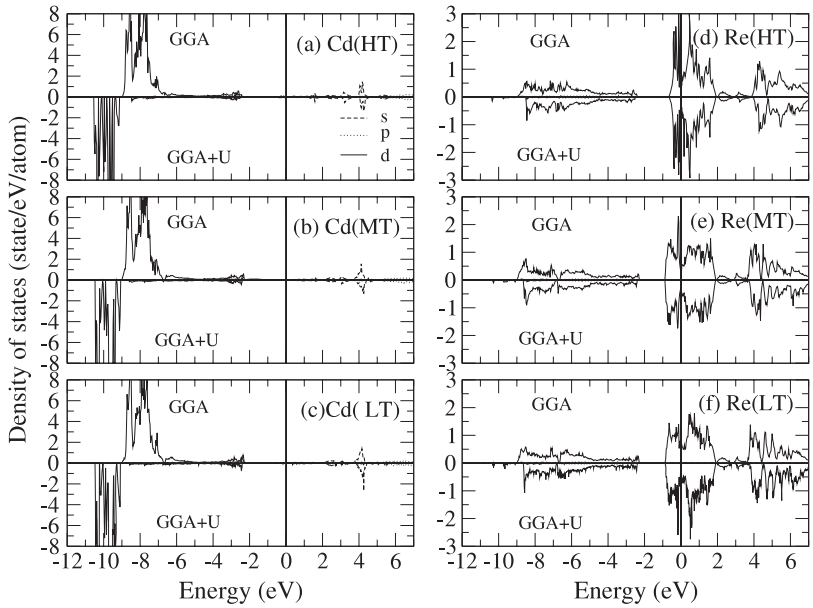

Figure 3. Partial DOS of Cd (left panels) ((a)–(c)) and Re (right panels) ((d)–(f)) of high-T (top panels), middle-T (middle panels) and low-T (bottom panels) from GGA and GGA + U.

in the Re t_{2g} bands not only in bandwidths but also in band dispersions due to the minor changes in the lattice structures. The T-dependent band dispersion discussed below varies in a subtle manner since the lattice distortions are indeed small. Therefore the overall DOS profile remains similar for all three phases. This is to be compared with the significant change in XAS data at low-T reported in a recent work [34]. Further investigations would clarify this issue.

Spin-decomposed Re DOS for high-, middle- and low-T phases from GGA and GGA + U are presented in figure 4. It can be seen that the Re t_{2g} band shows more sharp features in the high-T cubic phase than in the middle- and low-T tetragonal phases. This is presumably a natural consequence of the symmetry transition from cubic to tetragonal in which a large number of degenerate bands in the highly symmetric cubic phase split themselves and therefore result in smoother band shapes and larger bandwidths in the tetragonal phases of lower symmetry. As shown in figure 4, the lower bound of the Re t_{2g} band of the high-T phase is ∼0.2 eV higher than those of the other two phases at about 0.8 eV below Ef, while the upper bounds of the three phases are about the same at ∼1.9 eV above Ef. A similar spectral weight shift has been observed in a PES

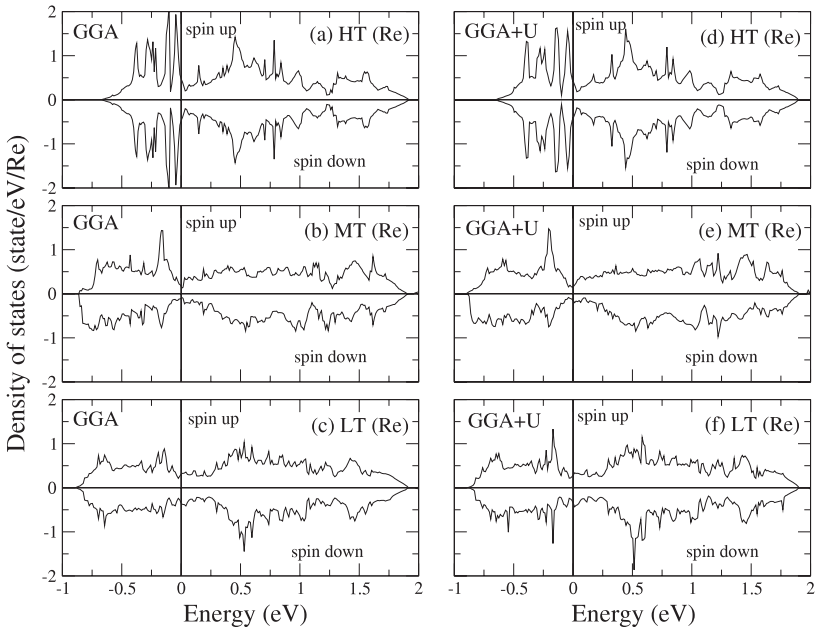

Figure 4. (a) Spin-decomposed DOS of Re around Ef for high-T (top panels), middle-T (middle panels) and low-T (bottom panels) from GGA (left panels) and GGA + U (right panels).

Table 2. Spin (M_s) and orbital (M_o) magnetic moments (μ_B/atom) of Re in $Cd_2Re_2O_7$ for high-, middle- and low-T phases from GGA + U.

	$\langle\lvert M_s\rvert\rangle$	$\lvert\langle M_s\rangle\rvert$	$\langle\lvert M_o\rvert\rangle$	$\lvert\langle M_o\rangle\rvert$
High-T	0.00	0.00	0.00	0.00
Middle-T	0.02	0.01	0.11	0.10
Low-T	0.01	0.00	0.01	0.00

measurement [26] that the highest intensity energy at 300 K is ∼0.2 eV higher than that at 5.3 K.

For the high-T phase, the Fermi level lies on the shoulder of the highest occupied spike, giving rise to a higher DOS of ∼0.9 state/eV/Re, whereas the DOS at Ef are significantly suppressed to ∼0.5 and ∼0.7 state/eV/Re for middle- and low-T phases, respectively. The obtained DOS reduction at Ef through the phase transition is consistent with the observation from NMR, susceptibility and specific heat experiments that DOS near Fermi surfaces decreases by ∼30 or ∼40% during the phase transition [12, 21, 22], though a recent PES work [34] shows a higher intensity at 20 K and similar intensities at 150 and 250 K around Ef. Another significant phenomenon is that, in contrast to the nonmagnetic ground state of the high-T phase, the spin-decomposed DOS turns into asymmetric for the other two phases, especially in the occupied part of the middle-T one, and hence give rise to nonvanished magnetic moments for the ground states. Actually the middle- and low-T phases exhibit not only spin but also orbital magnetic moments due to the spin–orbit coupling, as presented below.

The spin and orbital magnetic moments of Re from GGA + U are listed in table 2. Except for the truncation errors, the results from GGA are basically the same as those from GGA + U and therefore are not shown here. For the high-T phase, the averaged norm of spin $\langle|M_s|\rangle$ and orbital $\langle|M_o|\rangle$ moments as well as the norm of the averaged spin $|\langle M_s\rangle|$ and orbital $|\langle M_o\rangle|$ moments over the 8 Re ions in the tetragonal unit cell are all zero, indicating the nonmagnetic ground state. The middle-T phase shows some residual ferromagnetic spin moments of $\langle|M_s|\rangle = 0.02\ \mu_B$ along the crystal c axis with orientation fluctuations indicated by the much smaller value of $|\langle M_s\rangle| = 0.01\ \mu_B$. This local behavior (no long range order or weak long range order) could result from the frustrated lattice structure in which no spin direction is preferred for all the ReO_6 octahedra. The orbital magnetic moment is usually quenched in solids of the transition-metal oxides because of the dominant crystal field. Interestingly, due to the stronger spin–orbit coupling in 5d orbitals, Re ions show nontrivial ferromagnetic orbital moments of $\langle|M_o|\rangle = 0.11\mu_B$ along the c axis with slight fluctuations in orientation ($|\langle M_o\rangle| = 0.10\mu_B$). Why the frustrated structure does not destroy the unusual global orbital moment in the middle-T phase remains an open question. As for the low-T phase, the local moments $\langle|M_s|\rangle$ and $\langle|M_o|\rangle$ are both $0.01\mu_B$ with negligible global moments as presented in the table. The obtained total energies of the middle- and low-T phases in the magnetic ground state are ∼0.2 and ∼0.1 eV/f.u., respectively, lower than those in the nonmagnetic ground states. The local moment suggested in the susceptibility measurements [35], and the spin and orbital frustrations indicated in the NMR data [9, 12, 20], all refer to the same localized character as observed in the calculations. Experimentally, the nature of ferromagnetic interactions was confirmed in [21]. Furthermore, a large orbital susceptibility below 200 K was identified by means of a Cd Knight shift [22]. However, Re nuclear quadrupole resonance (NQR) spectra [8, 20–22] reveal no magnetic order in all three phases. This discrepancy between calculations and the experimental observation could be due to the nature of geometric frustrations in pyrochlore compounds. Meanwhile, the obtained small

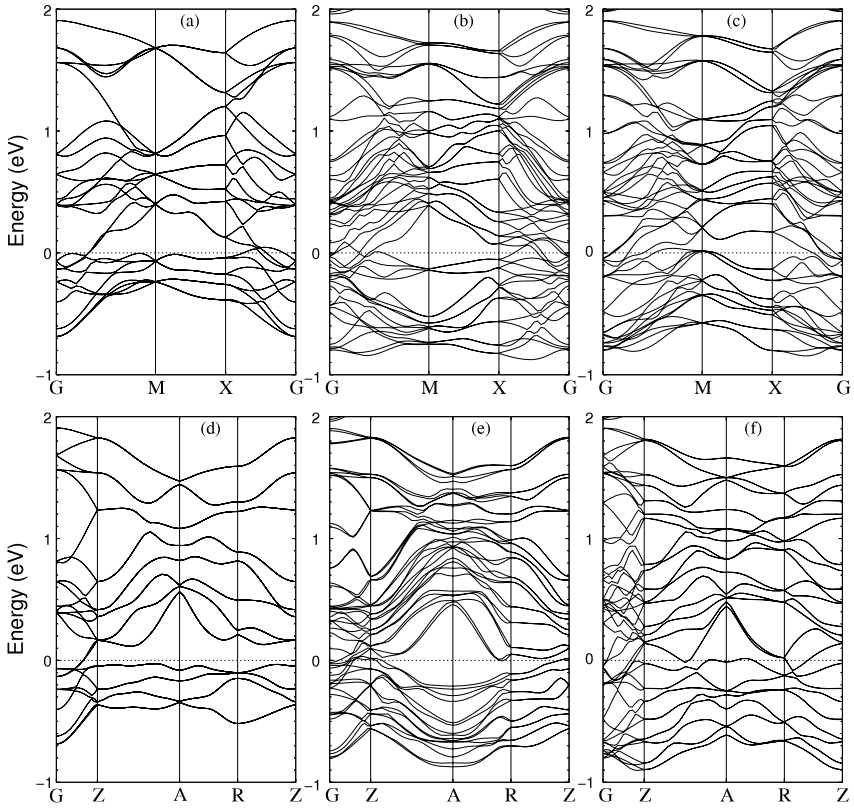

Figure 5. Band structures (Re t_{2g}) of $Cd_2Re_2O_7$ along high symmetry lines GMXG ((a)–(c)) and GZARZ ((d)–(f)) for high-T ((a) and (d)), middle-T ((b) and (e)) and low-T ((c) and (f)) phases from GGA + U.

magnetic moment at low T could be partially the reason why T_c of $Cd_2Re_2O_7$ is one order of magnitude lower than those of other pyrochlore superconductors. Further theoretical and experimental investigations would clarify these issues.

3.2. Band structure, Fermi surface, carrier number and Hall coefficient

Figure 5 shows the band structures of $Cd_2Re_2O_7$ for the three phases along the high symmetry lines GMXG and GZARZ in the tetragonal Brillouin zone from GGA+U. Since there exists no noticeable differences between the GGA and GGA + U band structures in this energy interval (Re t_{2g} band) for all three phases, we present only the GGA + U results here. With the spin–orbit coupling included, the inversion symmetry breaks down even in the high-T cubic phase [24]. Due to the higher cubic symmetry of the high-T phase, all 12 bands along MX, ZA, AR and RZ are fourfold-degenerate, while the 24 bands are doubly degenerate along GM, XG and GZ. On transition to the lower tetragonal symmetry, the degenerate bands split into much more complicated structures. For the middle-T case, the 24 Re t_{2g} bands along MX and RZ remain to be twofold-degenerate, while the degeneracies are lifted along the other high symmetry lines, resulting in 48 bands. Although both the middle- and low-T phases are in the same tetragonal symmetry and exhibit the same number of 16 symmetry operators, as can be seen in figure 5, the band structures of the low-T phase show relatively higher degeneracy than those of the middle-T phase. Not only bands along the MX and RZ directions, but also bands along ZA and AR are doubly degenerate at low temperature. This is because that all the atomic positions of the middle-T phase can be generated using 13 of the 16 operators, while those of the low-T phase can be generated using only 12 of the 16 operators.

It has been reported that the Fermi surface is sensitive not only to the spin–orbit interaction [23, 24] but also to the deformation of the crystal lattice [24] upon the phase transition. Although the structural changes are considerably smaller, whether these small changes lead to significant effects on the electronic structure at Ef certainly deserves further theoretical investigations. However, there is no report to date on the electronic structural changes due to the lattice variations. It can be seen in figure 5 that the slight lattice changes do affect the band structures significantly, particularly at Ef. For example, the low-T phase exhibits some heavy hole sheets at the M point, while there is no band crossing Ef at the M points in both the high- and middle-T phases. Around the A point, there exist some electron pockets in the low-T phase, whereas no similar feature appears in the high- and middle-T phases. Experimental measurements have demonstrated that the Hall coefficient (R_H) is positive at room temperature and becomes negative in the low-T phase, though there is no consensus on the sign of R_H for the middle-T phases [8, 12]. Such intense changes of carrier properties are closely related to the dramatic deformations of the Fermi surfaces upon phase transitions, as discussed below.

The calculated Fermi surfaces (FSs) in the tetragonal Brillouin zone from GGA+U for high-T, middle-T and low-T

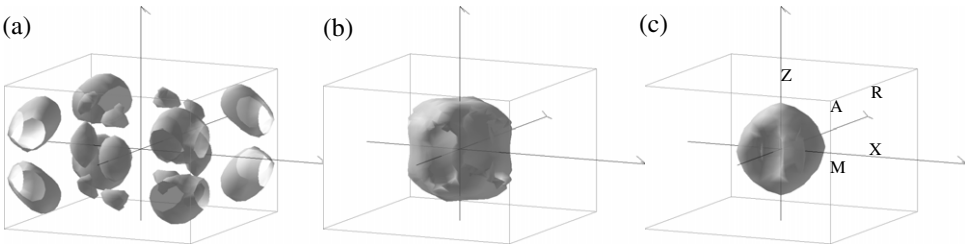

Figure 6. Fermi surfaces of the twofold-degenerate bands 367–368 (a), 369–370 (b) and 371–372 (c) of the high-T phase from GGA + U. (a) Band 367, (b) band 369 and (c) band 371.

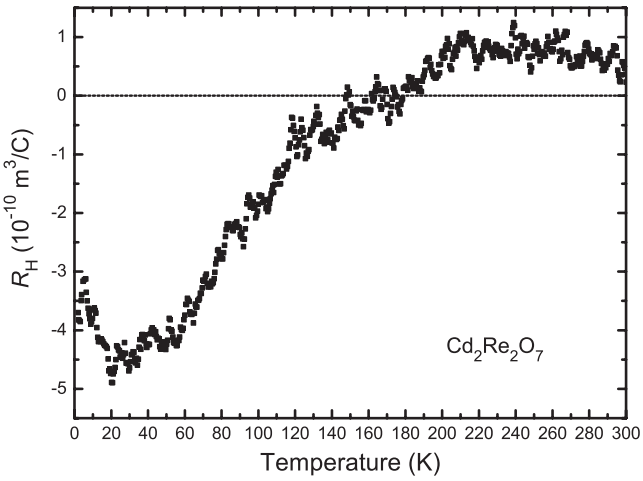

Figure 7. Temperature dependence of Hall coefficient (R_H).

phases are presented in figures 6, 8 and 9, respectively. Table 3 lists the calculated hole and electron numbers of each band with closed FSs for the three phases from GGA + U. The total hole and electron numbers as well as their differences are also tabulated for comparison. The temperature-dependent Hall coefficient R_H has been reported in both [8] and [12]. Nevertheless, there exist significant differences between these two reports. To clarify this issue, we also measured the Hall coefficient of $Cd_2Re_2O_7$. As shown in figure 7, R_H remains almost constant with a small positive value above 200 K. Below 200 K, R_H significantly drops to zero and remains negative in the middle-T and low-T phases. Overall, the results agree well with those from [8]. In the following, we discuss the carrier and related issues using the present R_H data. It is plausible that these drastic changes of the carrier properties are due to the deformations of the Fermi surfaces upon phase transitions. Since the Fermi surfaces (figures 6, 8 and 9), the carrier numbers (table 3) and the Hall coefficient (figure 7) are closely related to each other, we discuss them together below.

In the high-T phase, there are six bands crossing the Fermi level, leaving three distinguishable FSs due to the twofold degeneracy as shown in figure 6. The hole pockets of bands 367 and 368 centered at the cubic (fcc) high symmetry point K and the electron pockets of bands 369–372 at the Γ point are consistent with those reported in [24]. The total number of high-T hole carriers is 0.059h/f.u. from bands 367 and 368, while the slightly larger total electron number

Table 3. The carrier numbers of the electron (e/f.u.) and hole (h/f.u.) pockets in high-, middle- and low-T $Cd_2Re_2O_7$ from GGA + U. The total hole (H) and electron (E) numbers and the differences (E − H) are also listed.

(/f.u.)	High-T	Middle-T	Low-T
Band 366			0.000 16h
Band 367	0.029h	0.000 91h	0.000 36e
Band 368	0.029h		0.000 36e
Band 369	0.024e	0.018e	0.022e
Band 370	0.024e	0.000 53e	0.0094e
Band 371	0.0089e	0.000 16e	0.000 53e
Band 372	0.0089e		0.000 031e
H	0.059h	0.000 91h	0.000 16h
E	0.066e	0.019e	0.033e
E − H	0.007e	0.018e	0.033e

is 0.066e/f.u. from bands 369–372 (table 3). Neglecting the mobility effect of the hole and electron carriers, the difference in carrier numbers of 0.007e/f.u. would have resulted in a negative Hall coefficient, which is of the opposite sign to the experimentally observed R_H for the high-T phase. This contradiction indicates a relatively larger mobility of the hole carriers than the electron ones. But since the difference in carrier numbers is small, the difference in mobilities could be small as well.

The band structure, Fermi surface and carrier number of $Cd_2Re_2O_7$ in the high-T phase have also been studied in [24]. By using the lattice structure from [18] with internal lattice parameter $x = 0.309$ in the LDA calculations, they obtained much smaller electron pockets at Γ point with a small total electron carrier number of 0.039e/primitive cell [24]. To resolve this discrepancy, we also calculated the carrier number using the same lattice structure [18] in LDA calculations. Since our obtained total electron carrier number of 0.034e/primitive cell is quite close to that from [24], we therefore conclude that the short Re–O bond lengths given from a smaller x would enhance the overlap between Re and O ions and hence magnify the Re t_{2g} band dispersions. Consequently, the electron sheets shift to a higher energy and result in smaller electron pockets at Γ and therefore smaller carrier numbers. Upon full geometry optimizations carried out in this work, the bond lengths and band dispersions are thus relaxed due to a larger x of 0.318, giving rise to larger pockets and carrier numbers (table 3).

Another interesting issue is whether or not $Cd_2Re_2O_7$ is a compensated semi-metal through all three phases. Based on LDA Fermi surface calculations with $x = 0.309$ [18], [24]

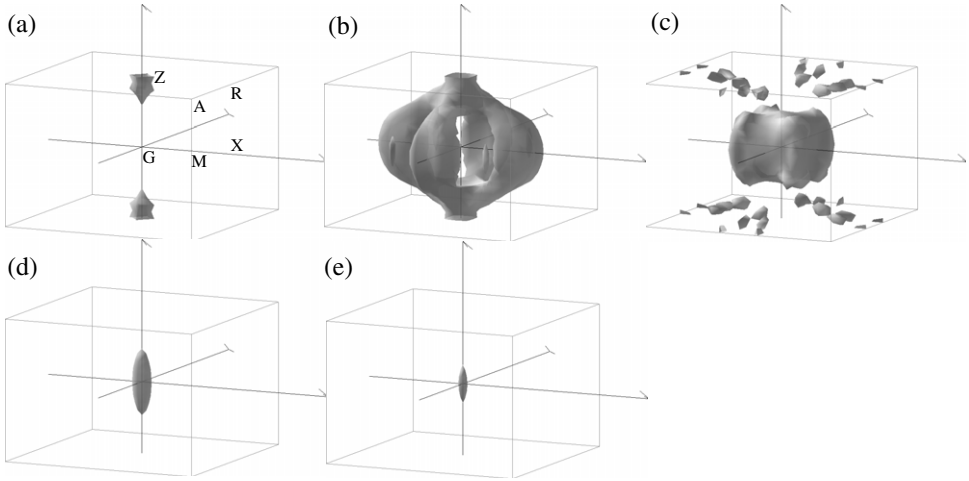

Figure 8. Fermi surfaces of bands 367–371 of the middle-T phase from GGA + U. (a) Band 367, (b) band 368, (c) band 369, (d) band 370 and (e) band 371.

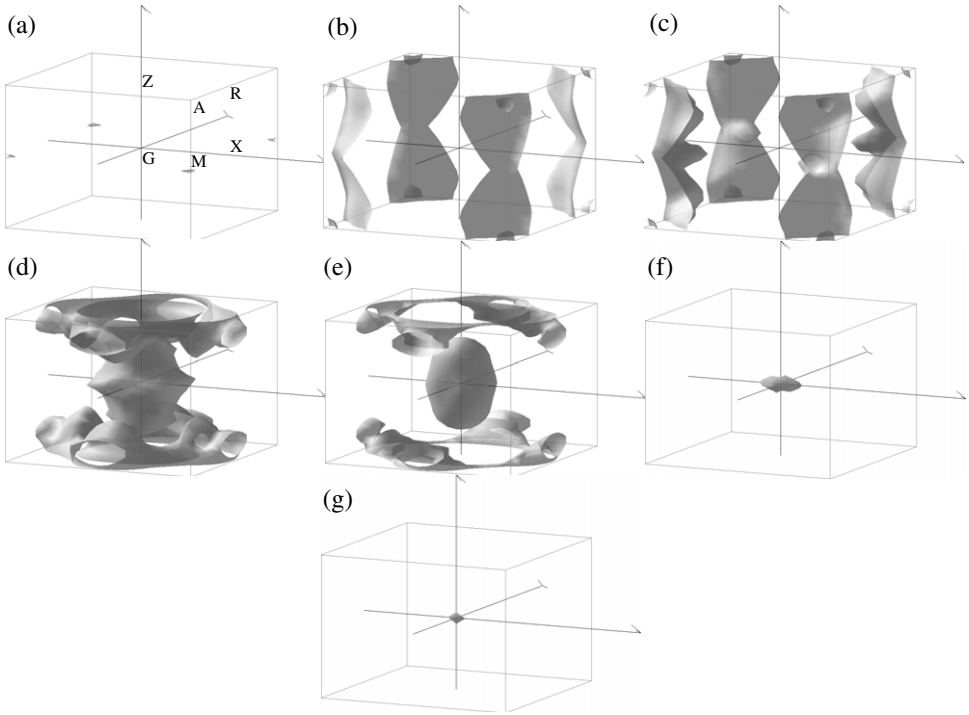

Figure 9. Fermi surfaces of bands 366–372 of the low-T phase from GGA + U. (a) Band 366, (b) band 367, (c) band 368, (d) band 369, (e) band 370, (f) band 371 and (g) band 372.

found equal numbers of total electron and hole carriers in the high-T phase. Due to this previous work, $Cd_2Re_2O_7$ was generally considered as a compensated semi-metal [23, 24]. Under lattice relaxation, we obtain approximately equal numbers of total electron (0.066e/f.u.) and hole (0.059h/f.u.) carriers in the high-T phase (table 3). Although the band structures are quite complicated (figure 5) and there is actually very little chance for the numbers of hole and electron carriers to be exactly the same, the high-T phase could still be taken as an *approximate* semi-metal because of the similar numbers of electron and hole carriers. However, this is not the case for either the middle- or low-T phase. As would be discussed below, the hole carrier number decreases to nearly zero while the electron carrier number decreases by about 50–60% in both the middle- and low-T phases (table 3). Therefore the net electron carrier number increases towards a lower temperature (table 3). Further, supported by the T-dependent Hall coefficient observed in this work (figure 7) and in [8], we therefore conclude that $Cd_2Re_2O_7$ would not be a semi-metal in both the middle- and low-T phases (see the discussions below).

For the middle-T phase, the only hole component of 0.000 91h/f.u. at the Z point comes from band 367 (figure 8 and table 3). Band 368 results in an open FS along the crystal

c direction with four lobes circumventing the zone center. The band energy outside the FS is negative (occupied) and the one inside is positive (unoccupied). In comparison with figure 6, one can see that the hole pockets of bands 367 and 368 of the high-T phase drastically deform into a much smaller hole pocket and a lantern-like open orbital, respectively, in spite of the slight distortions in the lattice structure towards the middle-T phase. The major electron pocket centered at the Γ point and a bunch of scattered minor electron pockets of band 369 provide the main contributions to the total electron carriers of 0.019e/f.u.. The obtained net carrier number of 0.018e/f.u. for the middle-T phase is much larger than that for the high-T phase, indicating a relatively negative R_H in the middle-T phase, being consistent with the measured R_H (figure 7, [8]).

Band 366 of the low-T phase affords a negligible hole pocket at the M point (figure 9). The main contribution of the electron carriers comes from bands 369 and 370, in which each band owns a major ellipsoid-like electron pocket centered at the Γ point. The FSs of bands 369 and 370 are topologically identical: besides the electron pocket at zone center, there is an additional open orbital surrounding the Z point which could originate from the scattered electron pocket in band 369 of the middle-T phase. Together with the other minor electron pockets of bands 367 and 368 at the A point and of bands 371 and 372 at the Γ point, the total electron carrier number is 0.033e/f.u., which is much larger than that obtained for both high- and middle-T phases. Neglecting the possible mobility effect, the strong trend that the carrier character becomes significantly negative through the phase transition clearly provides a reasonable explanation for the observed transition in sign of the Hall coefficient. According to our calculations, the carriers are predominantly electrons at low T. This is consistent with the experimental results in figure 7 and in [8]. Future investigations on the carrier mobility would shed more light on this topic.

Surprisingly, we observed in the low-T phase that the open orbitals of bands 367 and 368 both show a quasi-two-dimensional cylinder-like FS along the M–A direction. Similar 2D-like FSs have also been observed in superconducting materials such as MgB_2 [36], Na_xCoO_2 [37] and $NbSe_2$ [38]. Even though the two 2D-like FSs of low-T $Cd_2Re_2O_7$ show noticeable warping along k_z, especially in band 368 near the M point, together with the potential FS nesting, they could be related to the superconductivity observed at ∼1 K [4–6]. Whether the superconductivity is associated with the 2D- or 3D-like FS is unclear at the present moment. It was suggested that the superconducting order parameter is nearly isotropic in $Cd_2Re_2O_7$ (e.g. in [21]). Further detailed investigations on the degree of isotropy of the superconductivity in $Cd_2Re_2O_7$ would help to clarify this important issue.

4. Conclusion

In this work, we perform x-ray diffraction measurements to determine the lattice structures of $Cd_2Re_2O_7$ in the high-, middle- and low-T phases. Experimentally, we also studied the electronic structure of the high-T phase using O K-edge x-ray absorption spectroscopy. The T-dependent Hall coefficient was also measured from 2 to 300 K. Based on the observed lattice structures, detailed band structure calculations for the three phases have been carried out using the GGA and GGA + U methods with spin–orbit interaction included in the self-consistent calculations. We found that the on-site U has negligible effects on the Re 5d band structures; therefore both GGA and GGA+U band energies agree well with the observed XAS spectrum measured at 300 K. On the other hand, the on-site U significantly lowers the Cd 4d band energy, giving rise to a better agreement with PES results. This clearly indicates the relatively itinerant Re 5d and localized Cd 4d electron characteristics. Furthermore, we found that the spin–orbit coupling leads to nontrivial spin and orbital magnetic moments for the middle-T phase. We also found that the calculated carrier numbers for the three phases are consistent qualitatively with the measured Hall coefficient. Finally, the low-T phase exhibits quasi-two-dimensional Fermi surfaces. The mystery of the relation between the 1 K superconductivity and the peculiar electronic structure in the low-T phase calls for further investigations.

Acknowledgments

This work was supported by the National Science Council of Taiwan and the MOE-ATU project. We also thank NCHC, NCTS and Dr R Eguchi for technical support. HTJ thanks C S Hsue and K D Tsuei for valuable discussions.

References

[1] Katsufuji T, Hwang H Y and Cheong S W 2000 *Phys. Rev. Lett.* **84** 1998
[2] Moritomo Y, Xu S, Machida A, Katsufuji T, Nishibori E, Takata M, Sakata M and Cheong S W 2001 *Phys. Rev.* B **63** 144425
[3] Velasco P, Alonso J A, Tissen V G, Marshall W G, Casais M T, Martínez-Lope M J, de Andrés A, Prieto C and Martínez J L 2003 *Phys. Rev.* B **67** 104403
[4] Hanawa M, Muraoka Y, Tayama T, Sakakibara T, Yamaura J and Hiroi Z 2001 *Phys. Rev. Lett.* **87** 187001
[5] Sakai H, Yoshimura K, Ohno H, Kato H, Kambe S, Walstedt R E, Matsuda T D, Haga Y and Onuki Y 2001 *J. Phys.: Condens. Matter* **13** L785
[6] Jin R, He J, McCall S, Alexander C S, Drymiotis F and Mandrus D 2001 *Phys. Rev.* B **64** 180503
[7] Hanawa M, Yamaura J, Muraoka Y, Sakai F and Hiroi Z 2002 *J. Phys. Chem. Solids* **63** 1027
[8] Hiroi Z, Hanawa M, Muraoka Y and Harima H 2003 *J. Phys. Soc. Japan* **72** 21
[9] Arai K, Kobayashi K, Kodama K, Vyaselev O, Takigawa M, Hanawaa M and Hiroi Z 2002 *J. Phys.: Condens. Matter* **14** L461
[10] Mandrus D, Thompson J R, Gaal R, Forro L, Bryan J C, Chakoumakos B C, Woods L M, Sales B C, Fishman R S and Keppens V 2001 *Phys. Rev.* B **63** 195104
[11] Urano C, Nohara M, Kondo S, Sakai F, Takagi H, Shiraki T and Okubo T 2000 *Phys. Rev. Lett.* **85** 1052
[12] Jin R, He J, Thompson J R, Chisholm M F, Sales B C and Mandrus D 2002 *J. Phys.: Condens. Matter* **14** L117
[13] Castellan J P, Gaulin B D, Duijn J van, Lewis M J, Lumsden M D, Jin R, He J, Nagler S E and Mandrus D 2002 *Phys. Rev.* B **66** 134528

[14] Huo D, Mitsuda A, Isikawa Y, Sakurai J, Sakai H, Ohno H, Kato M, Yoshimura K, Kambe S and Walstedt R E 2002 *J. Phys.: Condens. Matter* **14** L257
[15] Bae J S, Ko H K, Yang I S, Lee Y S, Noh T W, Jin R, He J and Madrus D 2006 *J. Korean Phys. Soc.* **48** 946
[16] Hiroi Z, Yamaura J I, Muraoka Y and Hanawa M 2002 *J. Phys. Soc. Japan* **71** 1634
[17] Lu C, Zhang J, Jin R, Qu H, He J, Mandrus D, Tsuei K D, Tzeng C T, Lin L C and Plummer E W 2004 *Phys, Rev.* B **70** 092506
[18] Donohue P C, Longo J M, Rosenstien R D and Katz L 1965 *Inorg. Chem.* **4** 1152
[19] Yamaura J I and Hiroi Z 2002 *J. Phys. Soc. Japan* **71** 2598
[20] Vyaselev O, Kobayashi K, Arai K, Yamazaki J, Kodama K, Takigawa M, Hanawa M and Hiroi Z 2002 *J. Phys. Chem. Solids* **63** 1031
[21] Vyaselev O, Arai K, Kobayashi K, Yamazaki J, Kodama K, Takigawa M, Hanawa M and Hiroi Z 2002 *Phys. Rev. Lett.* **89** 017001
[22] Sakai H, Kato H, Kambe S, Walstedt R E, Ohno H, Kato M, Yoshimura K and Matsuhata H 2002 *Phys. Rev.* B **66** 100509(R)
[23] Singh D J, Blaha P, Schwarz K and Sofo J O 2002 *Phys. Rev.* B **65** 155109
[24] Harima H 2002 *J. Phys. Chem. Solids* **63** 1035
[25] Wang N L, McGuire J J, Timusk T, Jin R, He J and Mandrus D 2002 *Phys. Rev.* B **66** 014534
[26] Eguchi R, Yokoya T, Baba T, Hanawa M, Hiroi Z, Kamakura N, Takata Y, Harima H and Shin S 2002 *Phys. Rev.* B **66** 012516
[27] Lin J Y *et al* unpublished
[28] Blochl P E 1994 *Phys. Rev.* B **50** 17953
Kreese G and Joubert D 1999 *Phys. Rev.* B **59** 1758
[29] Kresse G and Hafner J 1993 *Phys. Rev.* B **48** 13115
Kresse G and Furthmüller J 1996 *J. Comput. Mater. Sci.* **6** 15
Kresse G and Furthmüller J 1996 *Phys. Rev.* B **54** 11169
[30] Perdew J P and Wang Y 1992 *Phys. Rev.* B **45** 13244
[31] Anisimov V I, Zaanen J and Andersen O K 1991 *Phys. Rev.* B **44** 943
[32] Liechtenstein A I, Anisimov V I and Zaanen J 1995 *Phys. Rev.* B **52** R5467
[33] Solovyev I V, Dederichs P H and Anisimov V I 1994 *Phys. Rev.* B **50** 16861
[34] Irizawa A, Higashiya A, Kasai S, Sasabayashi T, Shigemoto A, Sekiyama A, Imada S, Suga S, Sakai H, Ohno H, Kato M, Yoshimura K and Harima H 2006 *J. Phys. Soc. Japan* **75** 094701
[35] Sakai H, Kato H, Kambe S, Walstedt R E, Ohno H, Kato M, Yoshimura K and Matsuhata H 2002 *Phys. Rev.* B **66** 100509(R)
[36] Mazin I I and Antropov V P 2003 *Physica* C **385** 49
[37] Zhang P, Luo W, Cohen M L and Louie S G 2004 *Phys. Rev. Lett.* **93** 236402
[38] Johannes M D, Mazin I I and Howells C A 2006 *Phys. Rev.* B **73** 205102